Crystal sizes in evolving silicic magma chambers

Ilya N. Bindeman* Department of Geology and Geophysics, University of Wisconsin, 1215 W. Dayton Street, Madison, Wisconsin 53706, USA

ABSTRACT

Crystal size distributions (CSDs) of quartz and zircon phenocrysts in individual pumice clasts from several voluminous ash-flow tuffs provide a quenched snapshot view of conditions in preclimactic magma chambers. A common feature of these CSDs is a concave-down, lognormal shape, in contrast to the reported linear CSDs in more mafic systems. This feature is interpreted to be a general result of surface-controlled, size-dependent growth by a layer nucleation in silicic magmas at low supersaturation. Specific CSDs may be important for interpreting nucleation and crystal-growth conditions and mechanisms in magmas erupted as large ash-flow tuffs and smaller-volume volcanic units, and for fingerprinting different magma batches (layers) in products of the same eruption.

Keywords: crystal size distribution, ash-flow sheets, acid extraction, quartz, zircon, caldera, silicic, nucleation.

INTRODUCTION

Crystal sizes (phenocrysts and microlites) in igneous rocks are important parameters for interpreting magma cooling conditions and mechanisms (Cashman and Marsh, 1988; Higgins, 1998; Marsh, 1998). Silicic volcanic and plutonic rocks show significant variations in crystal sizes and proportions within the same unit, although these phenomena are poorly understood. These variations have particular importance for studying zoned magma chambers with significant gradients in composition and crystal content. Most experimental and observational work on crystal size distributions (CSDs) has been in mafic magma systems, i.e., lava lakes, sills, and plutons. Eutectoid silicic magmas are more complicated because of multiple saturation with as many as 10 minerals and a fluid phase. The high viscosity of silicic melts, with its dependence on temperature (T) and f_{H_2O}, causes complex nucleation and growth kinetics in pressure (P)-T-X_{H_2O} space and high levels of supersaturation due to heat or volatile loss (e.g., Hammer and Rutherford, 2002).

A snapshot view of large, batholith-scale magma chambers that have undergone deep eruptive drawdown (several kilometers) is provided by voluminous ($\sim 10^3$ km^3) ash-flow tuffs (e.g., Wilson and Hildreth, 1997). In plutons and batholiths, near-solidus cumulus processes lead to overprinting of near-liquidus CSDs by coarsening and overgrowth (Higgins, 1998). Where detailed field and melt-inclusion information is available, each pumice clast in a tuff bears valuable chemical, isotopic, and P-T-X_{H_2O} information for each locus in the magma chamber (Anderson et al., 2000). Phenocryst sizes in pumice clasts are important petrogenetic parameters, but they have received little attention, despite widespread use of phenocrysts for isotope and trace element analyses.

In this paper I describe an acid (HF and HBF_4) technique to extract and quantitatively measure abundance of phenocrysts in individual pumice clasts, coupled with camera- and computer-assisted measurements of their length, width, and shape (Appendix[1]). CSDs of quartz and zircon are presented for several well-known voluminous ash-flow tuffs and small-volume lavas (Fig. 1; Table DR1, Appendix [see footnote 1]).

RESULTS

Digital imaging allows examination of the external morphology of a very large number of acid-extracted crystals. In particular, >6000 zircons, and >3000 quartz crystals have been examined for the work reported here. The data suggest predominantly independent crystallization of quartz and zircon from rhyolitic melts: only five quartz and two zircon aggregates were found; inclusions of magnetite and zircon in quartz occur in <~5% of the examined crystals and are volumetrically negligible. CSDs of quartz and zircon are plotted as the natural logarithm of population density versus crystal length (Fig. 1), as is often employed in crystallization studies (Randolph and Larson, 1988; Marsh, 1998, see Appendix [footnote 1]). On these graphs, linear crystal growth with homogeneous nucleation exponentially increasing in time should result in a linear CSD, such as commonly measured in more mafic igneous rocks (e.g., Cashman and Marsh, 1988). In contrast, samples exhibit similar-in-shape, concave-down CSDs that allow general conclusions on the crystallization of quartz and zircon from silicic magmas as well as conclusions that are specific to each eruptive unit and magma system.

Quartz phenocrysts in each sample range over one order of magnitude in size, typically from 0.15 to 3.2 mm, and their mean and median sizes vary from 0.3 to 1.4 mm (Table DR1; see footnote 1). Regardless of size or sample, quartz has bipyramidal to near-spherical, poorly faceted morphology; crystal fragments surrounded by glass are also present. The lack of small (<0.1 mm) phenocrysts and microlites (confirmed in thin sections) and the deficiency of 0.15–0.8 mm quartz crystals for most samples yield concave-down CSD profiles with left-side truncation, and skewness toward larger crystal sizes (Fig. 1). The earlier-erupted, crystal-poor, and silica-richer parts of ignimbrites of several large, caldera-forming eruptions contain smaller quartz crystals than the later-erupted, hotter parts (e.g., BT, LBT, and LCT in Fig. 1A). CSD profiles of small-volume intracaldera lavas of similar compositions typically contain larger proportions of smaller crystals, but also lack smallest quartz phenocrysts and microlites.

Zircons range in length from <20 μm to >300 μm, and are perfectly faceted, predominantly four-sided prisms with short terminations. Zircons from different samples yield remarkably similar length/width versus length relationships, and elongation changes from 1.3 to 2.1 as length increases from 50 to 200 μm. Both width and length of zircons exhibit similar concave-down CSDs, and CSDs of length are discussed here. On zircon CSD plots (Fig. 1B) there is also a deficiency of small (<50 μm) crystals, and few <10 μm zircons were observed. The CSDs of zircons, HF extracted from magnetite and from quartz-feldspar mixtures, were measured in three samples (YL-4, LCT-A, and HRT-A), but yielded similar CSDs with a deficiency of large zircons; the proportion of zircons included in other phenocrysts is estimated as <10%. Concave-down CSDs have been described in metamorphic (Kretz, 1966; Carlson, 1999) and plutonic rocks (Higgins, 1998). Reported CSDs of zircons extracted through the conventional mechanical separation procedures (Poldervaart, 1956; Bindeman and Valley, 2001, 2002) are also concave-up, showing that the latter technique is also robust and generates roughly similar, but more scattered CSDs.

Particle concentration (number of crystals per cubic centimeter of vesicle-free magma)

*E-mail: inbindem@geology.wisc.edu.

[1]GSA Data Repository item 2003044, Table DR1, measured abundance, concentration, and sizes of phenocrysts, and Appendix, methods, is available from Documents Secretary, GSA, P.O. Box 9140, Boulder, CO 80301-9140, editing@geosociety.org, or at www.geosociety.org/pubs/ft2003.htm.

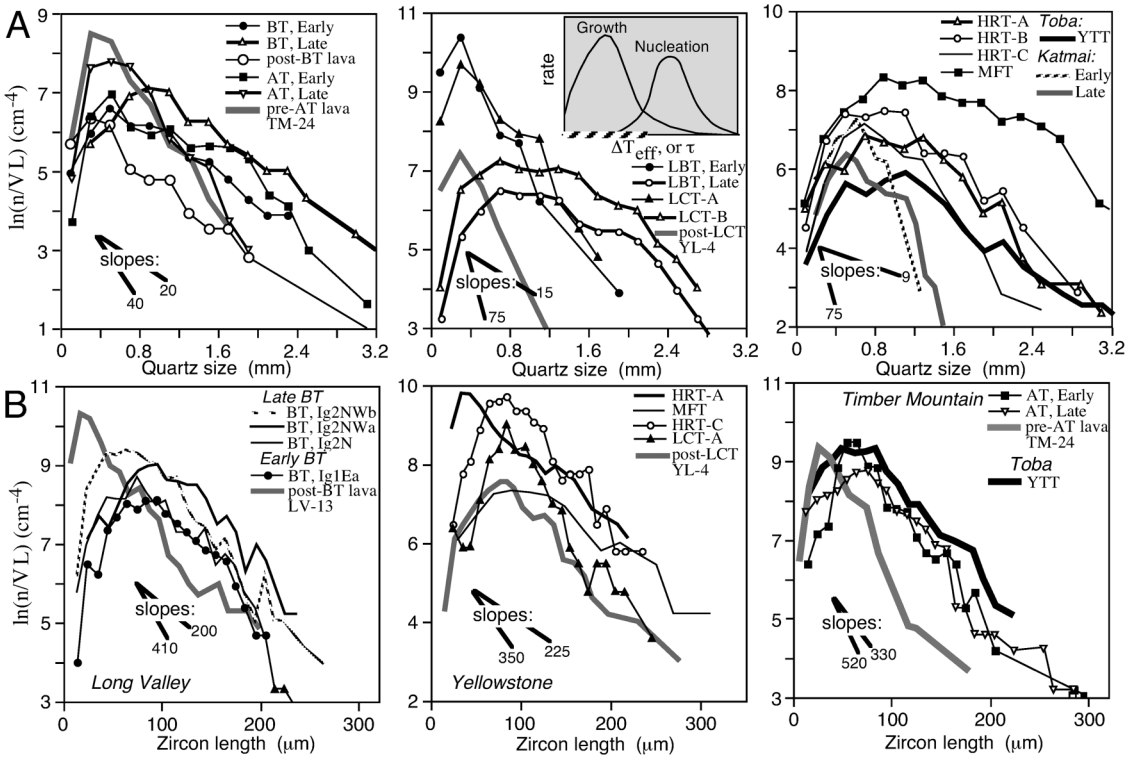

Figure 1. Crystal size distributions (CSDs) in several large ash-flow tuffs and in smaller-volume intracaldera lavas. A: Acid-extracted quartz phenocrysts. B: Acid-extracted zircon phenocrysts. Tuffs: LBT—Lower Bandelier, BT—Bishop; LCT—Lava Creek; HRT—Huckleberry Ridge; MFT—Mesa Falls; AT—Ammonia Tanks; YTT—Youngest Toba; see Table DR1 and Appendix (see text footnote 1). Each CSD is based on measurements of 150–400 quartz and 250–700 zircon crystals. Lack of smallest phenocrysts and microlites for large-volume tuffs is important, and suggests no new volume nucleation, or dissolution, prior to eruption. Slopes are shown and should yield 2–8 times shorter residence times (τ) at constant growth rates (G), according to simplified Avrami equation $d\ln(n)/dL = -1/G\tau$ (Cashman and Marsh, 1988). There is no simple correlation between CSD slope and eruptive volume. Inset on second diagram in A shows calculated nucleation and growth rates using equations 6.115 and 6.116 of Lasaga (1998), based on Avrami equation, but assuming time-variable nucleation and growth rates. Note that nucleation curve peaks at greater supersaturation (ΔT_{eff}) than growth curve, and that there is 0 nucleation but finite growth at small values of supersaturation (ΔT_{eff}), which is assumed linear with τ. Differing CSD shapes and slopes of quartz and zircon can be explained by variations of shape of nucleation and growth curves without changing their relative position. Hachured bar indicates possible range of small supersaturation ΔT_{eff} characteristic for studied silicic systems. Maximum ΔT_{eff} values are possible near chamber's walls.

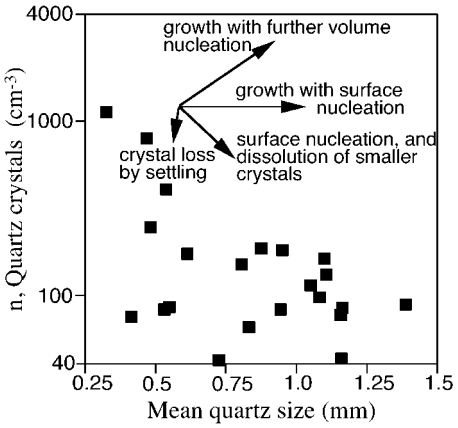

Figure 2. Correlation of particle abundance with mean size of quartz crystals. Each point represents measured parameters (Table DR1; see text footnote 1) for different samples; they contain quenched preeruptive crystal size distributions on various stages of growth that enable comparison as if they were representing a series of natural experiments at various P-T-X_{H_2O} conditions. Decrease in particle concentration with increasing crystal size demonstrates predominance of surface nucleation (with episodes of dissolution-reprecipitation of smaller crystals), and is too dramatic to be explained by crystal settling or any post-crystallization ripening process.

ranges from 4×10^1 to 10^3 for quartz and from 3×10^1 to 3×10^2 for zircon, but correlates negatively with quartz (and zircon) mean size (Fig. 2). However, there is a positive correlation between volume abundance of crystals and their mean size, because more phenocryst-rich samples tend to contain larger quartz and zircon (Table DR1; see footnote 1). Particle concentration and mean size of a CSD enable calculations of interparticle distance of 0.5–2 mm between neighboring quartz and 1.3–3.5 mm between zircon crystals.

CSDs are used to calculate population residence times if linear growth rates are assumed, or to estimate growth rates if the cooling time is known (e.g., Marsh, 1998). The right sides of CSDs in Figure 1 yield slopes that differ only by a factor of 2–8, although large-volume systems generally show flatter slopes for quartz than smaller-volume rhyolites. At homogeneous nucleation and similar-rate linear growth, such slopes should result in only 2–8 times longer residence times for large-volume rhyolites. However, geochronologic data on phenocrysts from large silicic magma bodies suggest far longer residence times and smaller growth rates (e.g., 3×10^5 yr and 10^{-15} cm/s for quartz, respectively; Christensen and DePaolo, 1993).

Herein I discuss CSDs of zircons that were earlier dated by ion microprobe: BT (Reid and Coath, 2000; Reid et al., 1997), LCT, MFT, and HRT (Bindeman et al., 2001) (see Fig. 1). U-Pb ages of zircons in large-volume tuffs that show less-steep CSD slopes are within analytical uncertainty of Ar-Ar sanidine eruption age, suggesting that zircons grew shortly prior to eruption. Paradoxically, smaller-volume Bishop intracaldera lava (sample LV-13), which shows the steepest slope (shorter implied residence time), was determined by Reid et al. (1997) to have resided in the magma chamber for >200 k.y. In addition, in the 0.5 Ma Yellowstone intracaldera rhyolite (sample YL-4), most zircons are derived from 2.4–0.7 Ma rhyolites (Bindeman et al., 2001). However, this small-volume lava shows steeper slopes on CSD graphs of quartz and zircon, consistent with shorter residence times. These observations suggest that CSDs are rejuvenated by overgrowth despite significant inheritance. As shown in Figure 1 (inset) and discussed in the next section, the observed CSDs cannot have been generated by a constant rate growth. In addition, contrary to exponentially increasing nucleation with time, a deficiency (or lack) of small crystals on CSD graphs suggests subdued nucleation, and Figure 2 demonstrates that the number of crystals per cubic centimeter decreases with increase in crystal mean size.

DISCUSSION

This study shows that silicic magmas exhibit rather similar concave-down CSDs of quartz and zircon, deficiency of smaller crystals, and almost no crystals smaller than a threshold size. Qualitative inspection of feldspar phenocrysts indicates that they lack small crystals and thus should have similar concave-down CSD profiles. This finding may be a common and previously unappreciated phenomenon of size distributions in silicic rocks. It characterizes large-volume magma chambers as well as small-volume domes and lavas. It is observed in both a major phenocryst phase (quartz) and an accessory phase (zircon) and warrants general explanation. Here I evaluate whether concave-down CSDs are related to (1) the intrinsic property of phenocryst growth from silicic magmas at small degrees of supersaturation, (2) postcrystallization ripening (e.g., Ostwald) phenomena, or (3) gravitational crystal redistribution.

Surface-Controlled Crystal Growth and Concave-Down, Lognormal CSDs

Crystals grow when there is supersaturation. In near-eutectoid silicic magmas, supersaturation is not likely due to temperature drop, but either to heat withdrawal or to volatile loss accompanying pressure release (e.g., Hammer and Rutherford, 2002). The degree of supersaturation in large silicic magma chambers may be governed by volatile loss or by addition of non-H_2O fluid (e.g., CO_2) if the system is water saturated, as are many shallow silicic systems (e.g., Anderson et al., 2000). Viscous silicic magmas require proportionally greater supersaturation to nucleate and grow phenocryst-size crystals than do mafic magmas, a simple result of the Stokes-Einstein relationship (Lasaga, 1998). In large silicic magma bodies such as produced the Bishop Tuff, cooling is slow, because such systems often exist for $>10^5$ yr, and quartz growth rates may be four orders of magnitude slower (10^{-15} cm/s; Christensen and DePaolo, 1993) than those measured in experiments (Swanson, 1977). For such slow growth rates and low degrees of undercooling, homogeneous nucleation rates are theoretically 0, because it takes a finite energy to form a nucleus (Tammann, 1898; Kirkpatrick, 1975; Lasaga, 1998). In practice, heterogeneous nucleation may be >0 because of the presence of other phases. Nucleation of quartz on the surface of existing quartz phenocrysts is well known from experiments (Swanson and Fenn, 1986). At high cooling rates (in experiments and nature), quartz does not form microlites, but rather fibrolitic spherulites with feldspar in near-eutectic proportions. At low cooling rates, quartz apparently does not nucleate on other phenocrysts (as is seen in this study) or gas bubbles (Swanson, 1977), but only on surfaces of preexisting quartz crystals. Zircons occur in all other crystals and may precipitate in their boundary layers (Bacon, 1989), although this is volumetrically insignificant (see previous section). Even at higher degrees of supersaturation in smaller-volume rhyolites, crystallization by crystal growth and interfacial attachment is seen here to dominate over nucleation.

The measured CSDs of quartz and zircon (Fig. 1) are lognormal, as can be demonstrated by the application of χ^2, Smirnov-Kolmogorov, and log-log cumulative frequency tests (Appendix; see footnote 1) at $>10\%$ confidence level (1% is enough to pass the lognormal test, Crow and Shimizu, 1988). On mathematical grounds, the lognormal CSDs could suggest (e.g., Crow and Shimizu, 1988; Appendix [see footnote 1]) (1) crystal growth proportional to their size, according to: $X_{J+1} = X_J + \varepsilon X_J$, where X is the size and ε is each small and random increment of growth J; and/or (2) fragmentation of larger crystals in the magma chamber. The size-dependent growth, noted by Marsh (1988), could find physical explanation if it is surface controlled (Eberl et al., 1998). A statistical approach of Eberl et al. (1998) allows fitting curves pertinent to various mechanisms of growth, i.e., homogeneous volume nucleation, surface nucleation, Ostwald ripening, and supply-controlled growth. The best overall fit to data points is provided by a model of surface-controlled growth (quartz) and surface-controlled growth with minor ($<5\%$ crystal volume) Ostwald ripening (zircon), followed by supply-controlled growth with progressively decreasing ε. Ostwald ripening does not shift the mean size, but affects the left sides of zircon CSDs, making them steeper. Thus, only the smallest zircons (<20 μm) could be affected by ripening. For quartz, measured CSDs do not require a ripening process, which would lead to a far steeper decrease in the left side of CSDs. It is shown in experiments that for millimeter-size quartz in rhyolites, Ostwald ripening is negligible (Cabane et al., 2001).

Although physical mechanisms of size-dependent growth are discussed here, surface nucleation may promote faster growth for larger crystals because they sink faster and interact with more melt, and this may occur in steps, because episodes of dissolution (often seen in cathodoluminescence [CL] images) may alternate with periods of surface-controlled growth (Fig. 2). Calculated diffusion of silica and zirconia over <1–2 mm interparticle distances is fast even at 725 °C compared to slow growth rates of quartz ($<10^{-10}$ cm/s) at low supersaturation (Swanson, 1977). In general, in medium to large silicic magma bodies, crystal-surface dynamics (surface roughness) will be a rate-limiting step determining crystal growth (Lasaga, 1998). Surface dynamics also predict crystal shapes, which are dependent on crystal-melt surface energy that correlates to a crystal's latent heat of fusion (Jackson et al., 1967). The observed near-spherical and poorly faceted quartz is indicative of interface-controlled growth, such as characterizes experimental crystallization of quartz from silica melt, and is explained by the low surface energy of quartz (Kirkpatrick, 1975). For high-surface energy and latent heat of fusion mineral zircon, a faceted morphology is observed for both interface- and diffusion rate–limited growths.

Fragmentation of phenocrysts in magma chambers into a random number of smaller and intermediate-size crystals (e.g., due to rupture of melt inclusions) is an additional proportionate mechanism that may generate lognormal CSDs, by analogy with sedimentology, and in accordance with Kolmogorov disaggregation theory (Appendix; see footnote 1). Breakage is evidenced by irregular and off-centered cores in CL images, often followed by crystallographic recrystallization. The lack of the smallest crystals proves that crystallization, and not dissolution, determined CSD and crystal morphologies prior to eruption.

The present work indicates that concave-down lognormal CSDs are an intrinsic property of near-equilibrium systems (such as large volume near-eutectoid silicic bodies). I demonstrate that crystal settling does not change the overall CSD shape and that CSDs can be used to fingerprint different magma batches and provide insights into (time integrated) crystallization in each magma system.

Magma Chamber Dynamics and CSDs

Magma chamber dynamics play a role in the modification of CSDs of crystals that are capable of quantitative redistribution by gravity. Crystal settling may be important when convection is sluggish, and crystals are lost downward at a rate that is proportional to r^2. Crystal settling can explain the lack of large crystals in the upper part of the magma body, and the gain of such crystals at the bottom, forming cumulate layers progressively richer in crystals, but these are rarely erupted. The general concave-down CSD shape is preserved even after $>50\%$ of the quartz volume has been removed or added (Fig. 3), because the less abundant large crystals constitute the most volume. Crystal settling would not explain the strong differences in quartz CSDs in the Lava Creek Tuff and Lower Bandelier Tuff (Fig. 1A), but is permissive for the Bishop Tuff (Fig. 3).

The alternative interpretation is that CSDs of earlier- and later-erupted parts of the same eruption represent two separate magma layers

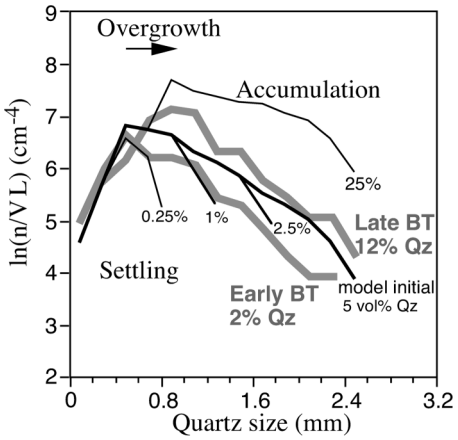

Figure 3. Calculated evolution of crystal size distributions (CSDs) of quartz as function of Stokes settling and accumulation in magma chamber. Modeling is done by dividing magma chamber into finite number of layers and by calculating net gain and loss of crystals in each layer through time. Initially CSD is same throughout magma chamber, e.g., because of convective stirring. Note that for CSD where significant quartz (Qz) volume percent is lost with few large crystals, general concave-up shape of CSD profile is preserved. Cumulative CSDs and quartz volume abundance of late and early Bishop Tuff (BT) are plotted for comparison. Additional crystallization of quartz by overgrowth during settling shifts CSD mean to right. It is permissive to explain CSDs in BT by crystal redistribution, as suggested by study of melt inclusions in quartz (Anderson et al., 2000).

or batches (Hervig and Dunbar, 1992). These batches (seen in LCT and LBT; see Fig. 1) originally resided at different depths in the magma chamber, had different supersaturation and/or growth conditions, but were juxtaposed by prior to eruption. Because zircon CSDs are not affected by crystal settling owing to small crystal size, they may fingerprint cooling and crystallization conditions from the *T* of zircon saturation to the *T* of eruption in each magma layer, or batch (Fig. 1B), that vary in Zr concentration and *T* (Table DR1; see footnote 1). Therefore, the initial diversity in CSD can be explained by different compositions and volatile contents of separate magma batches. Nonetheless, subsequent crystal growth is capable of rapidly reshaping CSDs, as is demonstrated by U-Pb dating of zircons. Therefore, CSDs reflect ''frozen-in'' conditions in the final preclimactic stage.

It is shown here that CSD studies of populations of several thousand crystals in centimeter-size pumice clasts provide an effective new tool for inferring preeruptive conditions of crystal growth, nucleation, and redistribution, and for fingerprinting different magma batches.

ACKNOWLEDGMENTS

I am grateful to A.T. Anderson for encouragement to write this paper, D. Eberl for suggestions on the Galoper software, C. Chesner for donating the Toba sample, J.S. Lackey and J. Fournelle for comments and electron microprobe help, and J.W. Valley, J. Hammer, C. Bacon, and an anonymous reviewer for insightful reviews. Supported by Department of Energy grant FG0293ER14389.

REFERENCES CITED

Anderson, A.T., Davis, A.M., and Lu, F., 2000, Evolution of Bishop Tuff rhyolitic magma based on melt and magnetite inclusions and zoned phenocrysts: Journal of Petrology, v. 41, p. 440–473.

Bacon, C.R., 1989, Crystallization of accessory phases in magmas by local saturation adjacent to phenocrysts: Geochimica et Cosmochimica Acta, v. 53, p. 1055–1066.

Bindeman, I.N., and Valley, J.W., 2001, Low-$\delta^{18}O$ rhyolites from Yellowstone: Magmatic evolution based on zircons and individual phenocrysts: Journal of Petrology, v. 42, p. 1491–1517.

Bindeman, I.N., and Valley, J.W., 2002, Oxygen isotope study of the Long Valley magma system, California: Isotope thermometry and convection in large silicic magma bodies: Contributions to Mineralogy and Petrology, v. 144, p. 185–205.

Bindeman, I.N., Valley, J.W., Wooden, J.L., and Persing, H.M., 2001, Postcaldera volcanism: In situ measurement of U-Pb age and oxygen isotope ratio in Pleistocene zircons from Yellowstone caldera: Earth and Planetary Science Letters, v. 189, p. 197–206.

Cabane, H., Laporte, D., and Provost, A., 2001, Experimental investigation of the kinetics of Ostwald ripening of quartz in silicic melts: Contributions to Mineralogy and Petrology, v. 142, p. 361–373.

Carlson, W.D., 1999, The case against Ostwald ripening of porphyroblasts: Canadian Mineralogist, v. 37, p. 403–413.

Cashman, K.V., and Marsh, B.D., 1988, Crystal size distribution (CSD) in rocks and the kinetics and dynamics of crystallization: II. Makaopuhi lava lake: Contributions to Mineralogy and Petrology, v. 99, p. 292–305.

Christensen, J.N., and DePaolo, D.J., 1993, Time scales of large volume silicic magma systems: Sr isotopic systematics of phenocrysts and glass from the Bishop Tuff, Long Valley, California: Contributions to Mineralogy and Petrology, v. 113, p. 100–114.

Crow, E.L., and Shimizu, K., 1988, Lognormal distributions: Theory and applications: New York, Dekker, 387 p.

Eberl, D.D., Drits, V.A., and Srodoñ, J., 1998, Deducing growth mechanisms for minerals from the shapes of crystal size distributions: American Journal of Science, v. 298, p. 499–533.

Hammer, J.E., and Rutherford, M., 2002, An experimental study of the kinetics of decompression-induced crystallization in silicic melt: Journal of Geophysical Research, v. 107, p. 1–24.

Hervig, R.L., and Dunbar, N.W., 1992, Cause of chemical zoning in the Bishop (California) and Bandelier (New Mexico) magma chambers: Earth and Planetary Science Letters, v. 111, p. 97–108.

Higgins, M.D., 1998, Origin of anorthosite by textural coarsening: Quantitative measurements of a natural sequence of textural development: Journal of Petrology, v. 39, p. 1307–1323.

Jackson, K., Uhlmann, D., and Hunt, J., 1967, On the nature of crystal growth from the melt: Journal of Crystal Growth, v. 1, p. 1–36.

Kirkpatrick, R.J., 1975, Crystal growth from the melt: A review: American Mineralogist, v. 60, p. 798–814.

Kretz, R., 1966, Grain-size distribution for certain metamorphic minerals in relation to nucleation and growth: Journal of Geology, v. 74, p. 147–173.

Lasaga, A.C., 1998, Reaction kinetics in geosciences: Princeton, New Jersey, Princeton University Press, 811 p.

Marsh, B.D., 1998, On the interpretation of crystal size distributions in magmatic systems: Journal of Petrology, v. 39, p. 553–599.

Poldervaart, A., 1956, Zircon in rocks: 2. Igneous rocks: American Journal of Science, v. 254, p. 521–554.

Randolph, A.D., and Larson, M.A., 1988, Theory of particulate processes (second edition): New York, Academic Press, 369 p.

Reid, M.R., and Coath, C.D., 2000, In situ U-Pb ages of zircons from the Bishop Tuff: No evidence for long crystal residence times: Geology, v. 28, p. 443–446.

Reid, M.R., Coath, C.D., Harrison, M.T., and McKeegan, K.D., 1997, Prolonged residence times for the youngest rhyolites associated with Long Valley caldera: ^{230}Th-^{238}U ion microprobe dating of young zircons: Earth and Planetary Science Letters, v. 150, p. 27–39.

Swanson, S.E., 1977, Relation of nucleation and crystal growth rate to the development of granitic textures: American Mineralogist, v. 62, p. 966–978.

Swanson, S.E., and Fenn, P.M., 1986, Quartz crystallization in igneous rocks: American Mineralogist, v. 71, p. 331–342.

Tammann, G., 1898, Uber die Abhangigkeit der Zajl der Kerne: Zeitschrift für Physik und Chemie, v. 25, p. 441–479.

Wilson, C.J.N., and Hildreth, W., 1997, The Bishop Tuff: New insights from eruptive stratigraphy: Journal of Geology, v. 105, p. 407–439.

Manuscript received 30 October 2002
Revised manuscript received 11 December 2002
Manuscript accepted 13 December 2002

Printed in USA

Data Repository Item: Table DR1: Abundance, concentration, and sizes of quartz and zircon phenocrysts

Tuff Sample	unit	pre-eruptive T (Qz-Mt) T °C	Zrc sat T °C	Crystal content vol%	Concentration SiO2 wt%	Zr ppm	Abundance Qz vol%	Zrc ppmv	n Qz cm^{-3}	n Zrc cm^{-3}	Mean size Qz um	Mean size Zrc um	Median size Qz um	Median size Zrc um	Measured number Qz	Measured number Zrc
Lower Bandelier (LBT), Toledo Caldera, NM, 600 km³ , 1.61 Ma																
LBT-10	Late	771		25	75		8.7		77		1156		1070		159	
LBT-4	Early	737		10	77		4.4		1129		326		265		242	
Bishop (BT), Long Valley Caldera, CA, 650 km³ , 0.76 Ma																
LV-27	Early	714	735	9	78	89	3.8	12	66	28	830	94	757	89	138	500
BC97-16	Early	754	735	9	78	89	2.1		73		738		635		179	
LV-751	Late	762	761	15	76	118	6.4	16	98	37	1084	88	1044	79	110	367
LV-748	Late	817	776	13	73	140	5.8	17	85	67	1164	99	1072	94	156	352
LV-3	Late	763	767	27	73	138	11.8	27	132	98	1110	78	1036	72	180	614
LV-13	lava		801	15	72	200	1.6	51	42	345	724	35	617	26	111	544
Lava Creek (LCT), Yellowstone Caldera, WY, 1000 km³ , 0.64 Ma																
LCT-3a, A	Early	800	809	11	78	187	7.8	14	780	37	472	95	380	89	318	304
LCT-4, B	Late	912	863	22	74	365	16.4		162		1099		1043		163	
YL-4	lava		882	9	76	393	2.0	70	61	325	343	84	297	80	238	430
Huckleberry Ridge(HRT), Big Bend Caldera, WY, 2500 km³ , 2.04 Ma																
HRT-3a, A	Early		863	19	77	328	9.8	25	113	108	1054	76	1019	59	257	342
HRT-1, B	Late		868	26	74	399	12.1		179		952		863		211	
HRT-C, C	Late		897	21	75	445	8.2	33	185	114	874	95	797	88	283	343
Mesa Falls (MFT), Island Park Caldera, ID, 300 km³ , 1.3 Ma																
MFT-1			800	37	78	168	18.5	49	88	41	1387	128	1302	114	283	307
Ammonia Tanks (AT), Timber Mountain Caldera, NV, 1000 km³ , 11.45 Ma																
TM-15	Early	762	809	14	76	215	7.0	22	83	67	948	84	757	76	206	637
TM-17	Late	870	842	20	73	293	2.9	16	171	47	617	77	565	71	209	508
TM-24	lava	754	776	7	76	135	2.3	8	241	125	486	42	437	37	167	160
Katmai-Valley of 10,000 Smokes rhyolite, AK, 8-12 km³ ,1912 AD																
KTM-3	Early		790	2	77.4	158	0.9		83		525		523		238	
Novarupta	Late	949	786	2	76.6	157	0.5		87		592		430		241	
Yongest Toba Tuff, Toba Caldera, Indonesia, 2800 km³ , 0.074 Ma																
YTT-102	Early	752	762	27	75.6	107	8.8	28	43	96	1150	75	940	69	166	404

*Oxygen isotope T (°C) estimates and sample descriptions are from Bindeman and Valley (2001, 2002)

n-measured particulate abundance (Fig. 1-2) per 1cc of melt; no zircons are found in Katmai samples, suggesting Tmagma>TZrc sat